THE JOURNAL OF PHYSICAL CHEMISTRY B

Article

pubs.acs.org/JPCB

From Ligand Fields to Molecular Orbitals: Probing the Local Valence Electronic Structure of Ni^{2+} in Aqueous Solution with Resonant Inelastic X-ray Scattering

Kristjan Kunnus,[†,‡] Ida Josefsson,[§] Simon Schreck,[†,‡] Wilson Quevedo,[†] Piter S. Miedema,[†] Simone Techert,[∥] Frank M. F. de Groot,[⊥] Michael Odelius,[§] Philippe Wernet,*[,†] and Alexander Föhlisch[†,‡]

[†]Institute for Methods and Instrumentation for Synchrotron Radiation Research, Helmholtz-Zentrum Berlin GmbH, Albert-Einstein-Str. 15, 12489 Berlin, Germany

[‡]Institut für Physik und Astronomie, Universität Potsdam, Karl-Liebknecht-Str. 24/25, 14476 Potsdam, Germany

[§]Department of Physics, Stockholm University, AlbaNova University Center, 10691 Stockholm, Sweden

[∥]Max Planck Institute for Biophysical Chemistry, Am Faßberg 11, 37077 Göttingen, Germany

[⊥]Department of Chemistry, Utrecht University, Universiteitsweg 99, 3584 CG Utrecht, Netherlands

Supporting Information

ABSTRACT: Bonding of the $Ni^{2+}(aq)$ complex is investigated with an unprecedented combination of resonant inelastic X-ray scattering (RIXS) measurements and ab initio calculations at the Ni L absorption edge. The spectra directly reflect the relative energies of the ligand-field and charge-transfer valence-excited states. They give element-specific access with atomic resolution to the ground-state electronic structure of the complex and allow quantification of ligand-field strength and 3d−3d electron correlation interactions in the $Ni^{2+}(aq)$ complex. The experimentally determined ligand-field strength is $10Dq$ = 1.1 eV. This and the Racah parameters characterizing 3d−3d Coulomb interactions B = 0.13 eV and C = 0.42 eV as readily derived from the measured energies match very well with the results from UV−vis spectroscopy. Our results demonstrate how L-edge RIXS can be used to complement existing spectroscopic tools for the investigation of bonding in 3d transition-metal coordination compounds in solution. The ab initio RASPT2 calculation is successfully used to simulate the L-edge RIXS spectra.

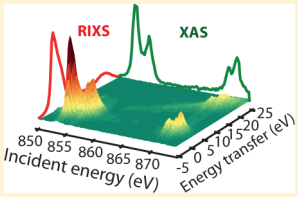

INTRODUCTION

3d transition metals in aqueous solution are interesting from a fundamental point of view as their hexaaqua complexes $[M(H_2O)_6]^{n+}$ represent the archetype of Werner complexes with coordinative bonding in octahedral symmetry.[1] Considering hydrogen bonding between the various coordination spheres of water molecules, they could even be regarded as chelate complexes,[2] and new insight into their electronic structure could help understanding the interplay of bonding, structure, and dynamics in these complexes. This in turn forms the basis for understanding their thermodynamic properties and reactivity, having implications for modeling and understanding phenomena ranging from water exchange reactions[3,4] to photochemical processes[5] and atmospheric liquid chemistry of 3d transition-metal ions in solution.[6]

While the structure of 3d transition metal (TM) ions and their complexes in aqueous solution can be addressed experimentally with numerous scattering and spectroscopic methods,[7] bonding can be assessed with a limited set of spectroscopic tools among which, historically, UV−vis spectroscopy has played a dominant role. Complementing such experimental results and due to the strongly polarized character of the coordinate bond, ligand-field theory[8,9] can be successfully applied to hexaaqua complexes. In particular, the dependence of the ligand-field (LF) state energies on ligand-field strength and 3d−3d Coulomb interactions for all $3d^n$ complexes were first calculated by Tanabe and Sugano in their seminal work from 1954.[10,11] The low-energy electronic excited state spectrum of a typical TM coordination complex can thus be described by, with increasing photon energy, the LF excitations, followed by the charge-transfer (CT) and ligand-centered excitations. At present, the excitations to LF states of octahedral TM complexes are very well understood at the semiempirical level of ligand-field theory. Today, ab initio calculations of the LF state energies pose a challenge as exact post-Hartree−Fock or advanced density functional theory (DFT) methods are required to correctly account for static and dynamic correlation effects. Further complications can arise for the calculation of higher-energy excited states such as the CT states. In addition, CT states of TM ions in solution are difficult to probe with UV−vis spectroscopy compared to LF states. Experimental difficulties arise because of higher transition energies which are well in the UV range and which often strongly overlap with very intense band gap excitations of the host. Thus, it appears

Received: October 10, 2013
Revised: November 28, 2013
Published: December 4, 2013

   dx.doi.org/10.1021/jp4100813 | J. Phys. Chem. B 2013, 117, 16512−16521

highly desirable to characterize bonding in aqueous TM ions in general and LF and CT state energies in particular with new experimental tools.

Soft X-ray spectroscopy offers a direct way for probing the valence electronic structure in an element-specific way.[12] It has the intrinsic property of being sensitive to a local charge distribution of a selected atomic site and therefore is ideally suited for studying charge-transfer, delocalization, and screening processes. Recently, several soft X-ray spectroscopic investigations of the electronic structure of 3d TM ions and compounds in solutions have been reported, based on X-ray absorption spectroscopy (XAS),[13−22] X-ray photoemission spectroscopy (XPS),[23−27] resonant photoemission spectroscopy (RPES),[24−27] and resonant inelastic X-ray scattering (RIXS) also known as resonant X-ray emission spectroscopy (RXES).[28−33] Note that RIXS in comparison to XAS and XPS is much less affected by core-hole effects.[34−37] In contrast to XAS and XPS, the resolution of the RIXS spectra is not limited by the core-hole lifetime broadening if subnatural line width excitation is employed.[38,39] RIXS is a type of Raman scattering, analogous to the widely used optical Raman scattering. In RIXS, the incident photon energy is scanned across the 2p core-level absorption edge of the TM, and the energy of the outgoing fluorescence photon is measured. The detected energy losses or energy transfers being the difference of incident and outgoing photon energies directly reflect the energies of the valence excitations. The final states in RIXS are identical to the final states of UV−vis absorption spectroscopy. In contrast to UV−vis spectroscopy, RIXS at the TM L-edge is sensitive to local charge distribution in an element-specific and symmetry-selective way. In addition, tuning the incident photon energy makes RIXS a truly two-dimensional spectroscopy, greatly increasing the information content compared to the UV−vis absorption spectroscopy. These features make RIXS a powerful tool for studies of low-energy excitations of complex systems,[34] therefore making up the added experimental complexity.

We investigate electronic structure of the hexaaqua complex $[Ni(H_2O)_6]^{2+}$ with measured and calculated Ni L-edge RIXS. We show how the X-ray spectroscopic results complement information from UV−vis spectroscopy. We have chosen Ni^{2+}(aq) for several reasons. First, as the Ni^{2+}−water interaction can be regarded as local and limited to only the first solvation sphere,[18] the system can be treated as an octahedral $[Ni(H_2O)_6]^{2+}$ Werner-type coordination complex. Second, with the Ni^{2+} $3d^8$ configuration, multiplet effects arising from core−valence interactions in the Ni^{2+} $2p^53d^9$ intermediate RIXS states are present but expected to be computationally feasible because of the comparably small number of states in contrast to TM ions with less filled 3d shells. The hexaaqua $[Ni(H_2O)_6]^{2+}$ complex is thus ideally suited to address the interplay of local atomic and intermolecular interactions in hexaaqua complexes. We note that Ni^{2+} compounds have been used before as a test case for XAS and RIXS spectroscopies.[40,41]

Currently the most successful computational scheme used to simulate the L-edge spectra of TM compounds is the crystal field multiplet (CFM) model developed by B. T. Thole and coworkers.[42,43] The CFM model is an implementation of the ligand-field theory and is thus semiempirical. Recently a number of theoretical developments have emerged looking for a more general and ab initio way to simulate L-edge XAS and RIXS spectra of TM compounds: hybrids of DFT and ligand-field theory,[44,45] 2-hole-2-electron time-dependent DFT,[46,47] DFT-CI,[48,49] and extended Bethe−Salpeter model.[50,51] Here we present the results of an ab initio RASPT2 computational scheme for L-edge RIXS, developed by Josefsson et al.[52] (A similar method was recently applied in refs 32, 33, and 53.). Our aim is to evaluate the performance and accuracy of the ab initio RASPT2 method with respect to experiment and the well-known CFM model. Note that the CFM model provides an accurate semiempirical description of the LF valence states and the core-excited $2p^53d^9$ states. Given the strongly polar Ni^{2+}−water bond, these are expected to dominate the XAS/RIXS spectra. Although for this relatively simple $[Ni(H_2O)_6]^{2+}$ complex the CFM model is sufficient, ab initio computational methods have a number of advantages. First, conceptually, an ab initio method provides maximum insight into the electronic structure (bonding, electron correlation) and the structure−spectrum relationship. Second, quantum chemistry methods like RASPT2 are implemented for calculations of any molecular system, thus enabling the modeling of systems with low molecular symmetry and/or with complicated or highly covalent bonding interactions, i.e., systems which are difficult to model within a semiempirical ligand-field theory framework like CFM.

METHODS

Experimental Details. $NiCl_2$ salt was purchased from Sigma Aldrich and used without further purification. The salt was solved in deionized water to a concentration of 0.5 mol/L. The dominant species at this concentration is the hexaaqua complex $[Ni(H_2O)_6]^{2+}$.[54,55]

The X-ray absorption (XA) spectrum was measured at the dipole beamline PM3 at the synchrotron radiation source BESSYII of the Helmholtz-Zentrum Berlin in Germany. The spectrum was recorded in transmission mode with a liquid transmission cell setup.[17] The excitation bandwidth was set to 0.4 eV. The photon energy was calibrated using the calibrated water pre-edge peak at 535 eV.

The RIXS spectra were measured at the beamlines U41-PGM and UE52-SGM at BESSYII. The experimental setup, FlexRIXS, utilizing an in-vacuum liquid jet for sample delivery was used for the measurements.[31] The diameter of the liquid jet amounted to 20 μm, matching the X-ray focus. The X-ray emission spectrometer is mounted at an angle of 90° from the incident X-ray propagation with the polarization of the incident radiation lying in the scattering plane (linear horizontal polarization) at U41. At UE52-SGM, the polarization of the X-ray radiation can be varied freely, and this was used to measure spectra with the polarization axis of the incident radiation both horizontal and vertical to the scattering plane. The excitation bandwidth at the Ni L-edge was set to 0.35 eV. The incident photon energy was calibrated with respect to the XA spectrum measured with the liquid transmission cell setup. The X-ray emission spectrometer was used in "slitless" mode using the jet as a source.[31] The resolution of the RIXS spectra was 1.2 eV (determined by the diameter of the jet). The emission energy scale was calibrated using elastically scattered light.

Computational Details. The ab initio RASPT2 calculations on $[Ni(H_2O)_6]^{2+}$ were performed using the MOLCAS software package.[56] The geometry of the $[Ni(H_2O)_6]^{2+}$ complex was optimized in the electronic ground state within D_{2h} symmetry at CASPT2 level with an active space consisting of the five nominally Ni 3d orbitals. ANO-RCC basis sets of

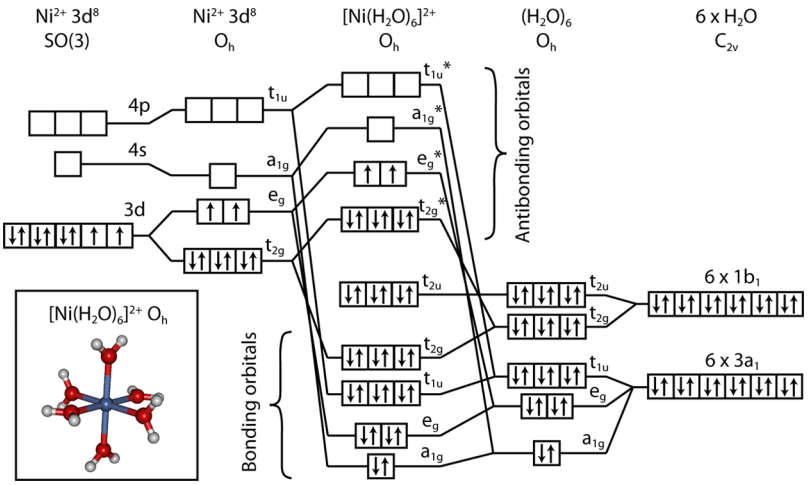

Figure 1. Schematic molecular orbital diagram for the hexaaqua $[Ni(H_2O)_6]^{2+}$ complex. Antibonding orbitals are marked with *. The calculated structure of the complex is shown in the inset. The orbital labels defined in the figure are used throughout the paper.

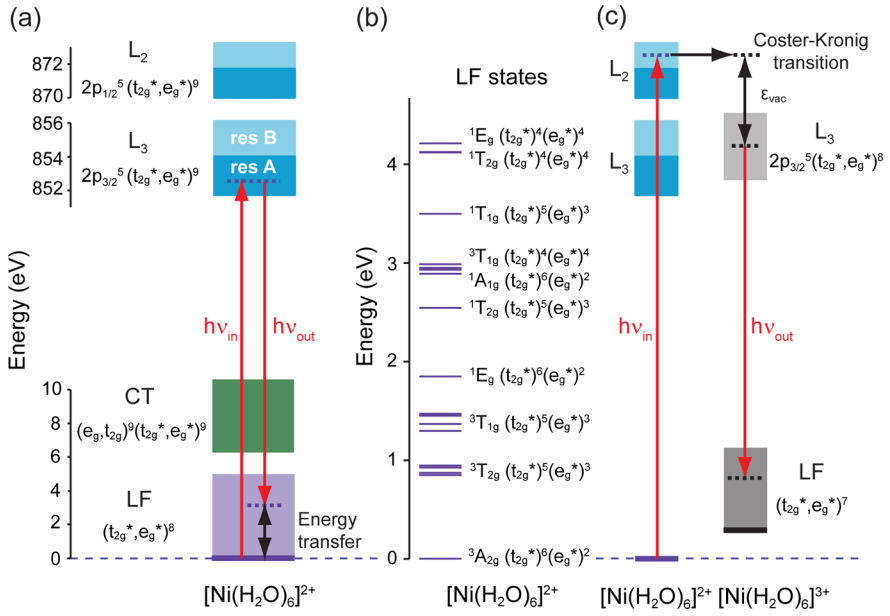

Figure 2. (a) Schematic representation of the relevant transitions and states in L-edge RIXS of $[Ni(H_2O)_6]^{2+}$ with approximate relative energies in eV. The filled boxes represent manifolds of closely lying states. The electron configurations of ligand-field (LF) and charge-transfer (CT) excited states and of the core-excited states at the L_3- and L_2-edges are given (the two X-ray resonances "res A" and "res B" are defined with Figures 3 and 4). (b) Calculated RASPT2 energy diagram of the LF states of $[Ni(H_2O)_6]^{2+}$ denoted by their respective term symbols (the highest-energy LF state $^1A_{1g}$ at 7.3 eV is out of the scale) and the corresponding strong-field orbital configurations (for more details of the orbital and spin compositions see the Supporting Information). (c) Schematic representation of a selected L_2-excitation undergoing a Coster–Kronig transition with ejection of an electron (with kinetic energy ε_{vac}) followed by a fluorescence decay with transition to an arbitrary LF state of $[Ni(H_2O)_6]^{3+}$. Note that the energy of the ground state of $[Ni(H_2O)_6]^{3+}$ is not drawn to scale with respect to the ground state of $[Ni(H_2O)_6]^{2+}$.

VTZP quality were used in the CASPT2/RASPT2 calculations.[57,58] Scalar relativistic effects were introduced via a spin-free Douglas–Kroll–Hess transformation.[59,60] According to the calculations, the complex is almost perfectly octahedral with a Ni–O distance of 2.080 Å.

Calculations of Ni 2p core-excited states and Ni 3d valence-excited states were performed at the RASPT2 level. RASSCF[61] states were calculated with 2p orbitals in the RAS1 subspace (one hole allowed) and 3d orbitals in the RAS2 subspace (all possible permutations allowed). Within each symmetry class in D_{2h}, the states were optimized in a state-averaged RASSCF procedure which was followed by a perturbative inclusion (PT2) of dynamical correlation.[62] Spin–orbit coupling was included using the RASSI technique.[63] Energies of the core-excited states were shifted by −1.9 eV to compensate for limitations in basis set and active space and match with the experiment. Energies of the valence excitations are presented as calculated.

For comparison we also simulated the RIXS spectra using the semiempirical CFM model. The ligand-field 10*Dq* parameter was set to 1.1 eV according to the experimentally determined value, and the atomic Slater integrals calculated at the Hartree–Fock level were scaled by a factor of 0.8.

For both the ab initio RASPT2 and the CFM calculations, RIXS spectra were simulated by multiplying absorption and emission transition moments without any interference effects

dx.doi.org/10.1021/jp4100813 | J. Phys. Chem. B 2013, 117, 16512–16521

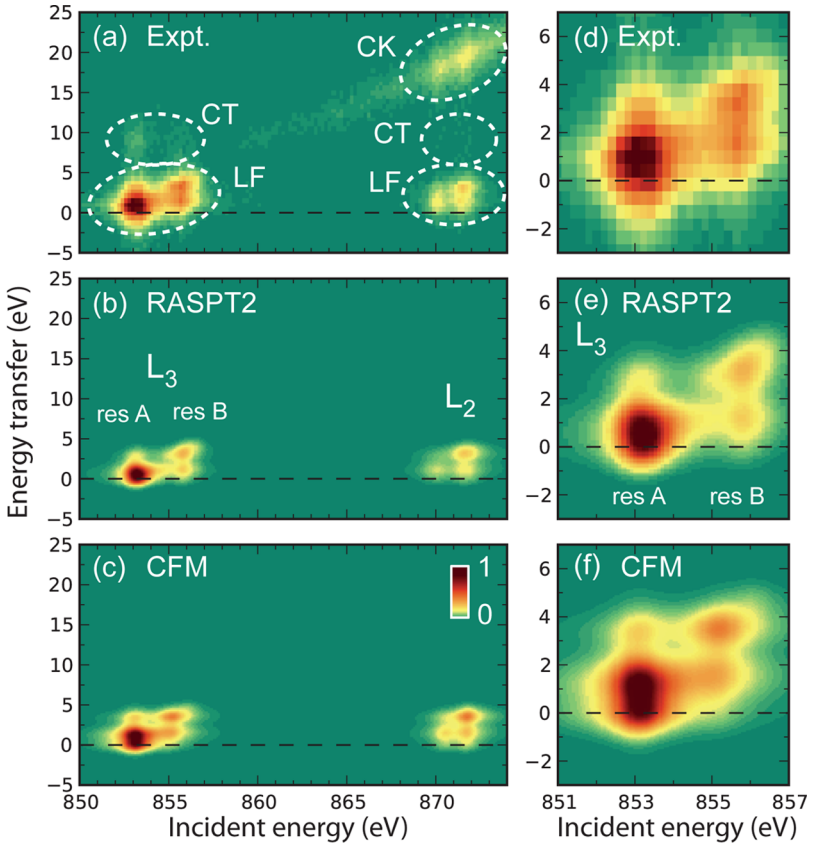

Figure 3. (a)−(c) Measured and calculated Ni L-edge RIXS maps of $[Ni(H_2O)_6]^{2+}$ with (a) experiment, (b) RASPT2 calculation, and (c) CFM calculation. Spectral features denoted with LF and CT correspond to ligand-field and charge-transfer excited states, respectively. The features denoted CK result from fluorescence decays preceded by Coster−Kronig decays [see schematic diagram in Figure 2c]. Panels (d), (e), and (f) are zooms into the LF features at the L_3-edge from experiment, RASPT2, and CFM, respectively. The intensities are normalized to one at maximum and encoded in the color.

included. The following convolution scheme was applied (values for the fwhm are given): 0.35 eV Gaussian broadening taking into account the excitation bandwidth, 0.5 eV (1.0 eV) Lorentzian lifetime broadening at the L_3 (L_2) edge for core-excited states, and 1.2 eV Gaussian broadening of RIXS spectra to account for the spectrometer resolution. An additional 0.5 eV Gaussian broadening of both XA and RIXS spectra was introduced to account for inhomogeneous broadening. No polarization effects were included in the simulation of the RIXS spectra (the calculated RIXS maps thus correspond to excitation with unpolarized light). This is justified as polarization effects on the valence-excited RIXS states were checked to be small (see the Supporting Information) and the Ni^{2+} partial-fluorescence yield XA spectrum derived from the RIXS spectra was shown before to exhibit negligible polarization effects.[64]

RESULTS AND DISCUSSION

The main frontier orbitals necessary to characterize the electronic structure of the $[Ni(H_2O)_6]^{2+}$ complex are also the ones probed by Ni L-edge RIXS, namely the nominal water bonding e_g and t_{2g} orbitals and the nominal Ni 3d antibonding e_g^* and t_{2g}^* orbitals (Figure 1). LF excitations involve only nominal Ni 3d orbitals and correspond to electronic transitions from the $^3A_{2g}$ $(e_g,t_{2g})^{10}(t_{2g}^*)^6(e_g^*)^2$ ground state to the final states of the $(e_g,t_{2g})^{10}(t_{2g}^*)^{6-n}(e_g^*)^{2+n}$ (n = 1, 2) configurations. They determine the optical properties of the complex in the UV−visible spectral region. CT excitations involve the nominal water orbitals and correspond to transitions from $^3A_{2g}$ $(e_g,t_{2g})^{10}(t_{2g}^*,e_g^*)^8$ to states of the $(e_g,t_{2g})^9(t_{2g}^*,e_g^*)^9$ configuration.

With the schematic depiction of the relevant transitions shown in Figure 2a, we explain how LF and CT states are probed with Ni L-edge RIXS. All energies are plotted with respect to the $^3A_{2g}$ ground state of $[Ni(H_2O)_6]^{2+}$. Absorption of a soft X-ray photon with incident energy $h\nu_{in}$ promotes the system to a core-excited state with a vacancy in the 2p shell and an additional electron in the unoccupied valence orbitals. The strongest 2p X-ray transitions in $[Ni(H_2O)_6]^{2+}$ occur to the antibonding t_{2g}^* and e_g^* orbitals. The 2p core-excited states in $[Ni(H_2O)_6]^{2+}$ are split by approximately 17 eV because of the 2p spin−orbit interaction separating the L_3-edge $[(2p_{3/2})^5(t_{2g}^*,e_g^*)^9$ configuration] and the L_2-edge $[(2p_{1/2})^5(t_{2g}^*,e_g^*)^9$ configuration]. The core-excited states can decay via fluorescence (note that ∼99% decay via Auger decay[65]), promoting the system back to the ground or to valence-excited states of $[Ni(H_2O)_6]^{2+}$. If the $h\nu_{out}$ is measured, the energy transfer $h\nu_{in} - h\nu_{out}$ can be determined, which in turn directly reflects the energy of the corresponding LF or CT final states (a RIXS transition to an arbitrary LF final state is shown in Figure 2a).

The energies of the LF states in $[Ni(H_2O)_6]^{2+}$ as derived from the RASPT2 calculations are plotted in Figure 2b. Altogether there are 45 states in the LF manifold which can be grouped into 11 terms (states within each term are degenerate in perfect octahedral symmetry and without 3d spin−orbit coupling). The question arises how these LF states can be

dx.doi.org/10.1021/jp4100813 | J. Phys. Chem. B 2013, 117, 16512−16521

probed in detail with Ni L-edge RIXS and how this compares to results from UV−vis absorption spectroscopy.

For this we inspect the measured and calculated Ni L-edge RIXS and XAS results displayed in Figures 3 and 4. The

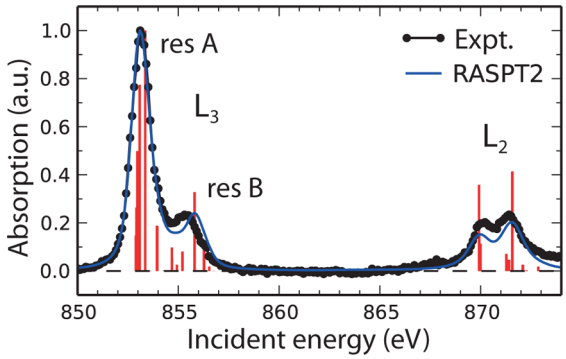

Figure 4. Measured (black circles) and calculated (RASPT2, solid blue line and red sticks representing single transitions) Ni L-edge X-ray absorption spectrum of $Ni^{2+}(aq)$. The experimental X-ray absorption spectrum was measured in transmission mode and published before in ref 52.

measured RIXS data (Figure 3a,d) are compared to the results of the RASPT2 (Figure 3be) and CFM (Figure 3c,f) calculations. We first note the overall very good agreement between experiment and calculations. This is emphasized by the zoomed-in view on the LF states in Figure 3d,e,f. Inelastic scattering features are apparent at the Ni L_3- and L_2-edges at incident photon energies of 851−857 and 869−874 eV, respectively. The most intense RIXS features at energy transfers of 0−5 eV at the L_3-edge correspond to the LF final states. The much weaker intensities at energy transfers of 6−12 eV correspond to ligand-to-metal CT final states. Note that these CT states are not included in the RASPT2 and CFM calculations, and accordingly the RIXS features are absent in the calculated RIXS maps in Figure 3b,c. The CT final states are excluded here for practical reasons; it requires more effort to accurately model both the LF and CT states than only the LF states. Note that the CT states nevertheless carry significant information about the electronic structure, especially related to the covalent orbital mixing. An attempt to model the CT states is made in an upcoming publication[66] in which we apply both CFM and ab initio RASPT2 methods to calculate the CT RIXS feature. For now we will focus on the LF states which are sufficient for discussion of ligand-field and 3d−3d Coulomb interactions (static electron correlation).

The last set of final states can be found at 12−22 eV and at the L_2-edge only. These intensities are due to a cascade process including a radiationless Coster−Kronig (CK) transition[67] as schematically depicted in Figure 2c and as discussed before for TM ions in solution in refs 19 and 30. Here the $2p_{1/2}$ core-excited states decay via a CK process upon electron ejection to $2p_{3/2}$ core-excited states of the $[Ni(H_2O)_6]^{3+}$ complex. These then decay radiatively to the valence-excited states of the $[Ni(H_2O)_6]^{3+}$ complex. In Figure 3 the corresponding features are labeled with CK. As shown in Figure 2c, the energy transfers of the CK features can be estimated from the $[Ni(H_2O)_6]^{2+}$ LF-state energies plus the Ni 2p spin−orbit splitting of 17 eV. Finally, we point out that the intensity of elastic scattering at an energy transfer of 0 eV is slightly overestimated in both calculations (compare Figure 3d,e,f). The intensity of elastic scattering depends on a number of factors such as the experimental geometry, polarization of the incident radiation, and sample surface shape and roughness. These effects are not included in the simulated RIXS spectra.

The agreement of measured and calculated spectra enables the determination of the ligand-field strength and 3d−3d Coulomb repulsion parameters, as will be discussed below, together with a detailed comparison of the two theoretical approaches.

Determination of Ligand-Field and Racah Parameters. As the same final states are reached with excitation at the L_3- and L_2-edge, albeit with smaller intensities at L_2, we focus in the following on excitations at the L_3-edge only. We denote the two clearly distinct resonances at the L_3-edge as resonance A at 853.2 eV and resonance B at 855.6 eV (Figures 3 and 4). States in resonance A have a dominantly triplet character (antiparallel spins of 2p and 3d hole), whereas states in resonance B have considerable singlet character (see also Figure S2 of the Supporting Information). RIXS spectra displaying intensities versus energy transfer at these two resonances (corresponding to vertical cuts through the maps in Figure 3) are presented in Figure 5. The peak at zero energy transfer in Figure 5a corresponds to transitions back to the ground state $^3A_{2g}$

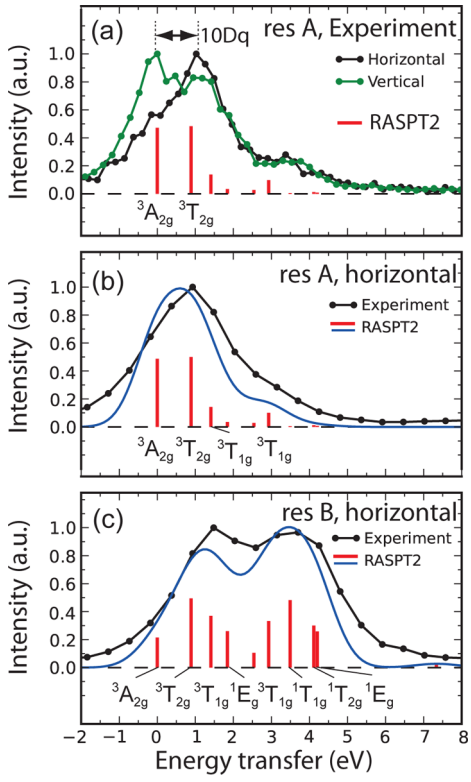

Figure 5. Measured and calculated Ni L_3-RIXS spectra of $[Ni(H_2O)_6]^{2+}$ in the energy-transfer region of the ligand-field (LF) features with (a) experimental spectra with excitation at resonance A (incident photon energy 853.2 eV) for horizontal (black) and vertical (green) polarization of the incident radiation (see Methods for details) and calculated LF peaks (RASPT2, red sticks, horizontal polarization). Panels (b) and (c) show experimental spectra (black circles and lines) with excitation at resonance A (853.2 eV) and B (855.6 eV), respectively, compared to the calculated spectra (RASPT2, blue solid lines). The sticks represent individual peaks with corresponding assignments of the LF states. The intensities are normalized to 1 at the maximum.

dx.doi.org/10.1021/jp4100813 | J. Phys. Chem. B 2013, 117, 16512−16521

(resonant elastic scattering). The intensity of the elastic scattering peak depends on the position of the detector with respect to the polarization plane of the incident radiation. It is enhanced if photons are detected normal to the polarization plane (vertical polarization of the incident radiation in our case, see Methods) as demonstrated in Figure 5a. The RIXS peak at a transfer of 1.1 eV corresponds to the $^3T_{2g}$ final state. The deduced peak energy separation of 1.1 eV with respect to the ground state equals the LF parameter $10Dq$.[9] A detailed comparison of calculated RASPT2 and measured RIXS spectra at resonances A and B is done with Figure 5b,c. This comparison demonstrates that by varying the incident photon energy the relative contributions of the various LF states can be varied in the RIXS spectra. At resonance B this enables us to extract the energy of the $^1T_{1g}$ state. The comparison of experimental and calculated values for the LF states are summarized in Table 1. The experimental LF state energies

Table 1. Measured and Calculated Energies of the Given LF States with Respect to the $^3A_{2g}$ Ground State[a]

	RIXS expt. this work (eV)	RASPT2 theory this work (eV)	CFM theory this work (eV)	RAS theory[68] (eV)
$^3A_{2g}$	0	0	0	0
$^3T_{2g}$	1.1	0.9	1.1	1.0
$^3T_{1g}$(F)	(1.4)	1.4	1.8	1.7
^1E_g(D)	–	1.8	1.9	2.2
$^1T_{2g}$(D)	–	2.5	2.9	3.1
$^1A_{1g}$(D)	–	2.9	3.2	3.5
$^3T_{1g}$(P)	3.4	2.9	3.4	3.6
$^1T_{1g}$	3.5	3.5	3.6	–
$^1T_{2g}$(G)	–	4.1	4.4	–
^1E_g(G)	–	4.2	4.5	–
$^1A_{1g}$(S)	–	7.3	7.8	–

[a]The measured energies result from peak fits to the experimental spectra shown in Figure 5 (see the Supporting Information, Figure S3 and Tabel S1). Because of insufficient resolution some of the LF states could not be resolved in the experiment. The calculated RASPT2 energies are averages for the given term. The calculated RAS energies are taken from ref 68.

were retrieved by peak-fitting the RIXS spectra in Figure 5 (see also the Supporting Information). The $^3T_{2g}$ and $^3T_{1g}$(P) state energies result accordingly from a fit to the RIXS spectrum measured at resonance A (Figure 5b and Figure S3c of the Supporting Information). The $^1T_{1g}$ state energy results from a fit to the RIXS spectrum measured at resonance B (Figure 5c and Figure S3d of the Supporting Information). Note that the lower-energy peak in the latter spectrum is a mixture of $^3T_{2g}$, $^3T_{1g}$(F), and ^1E_g(D) (see Figure 5c) and can therefore only tentatively be assigned to $^3T_{1g}$(F) (hence the parentheses in Table 1).

We note that in spite of the overall good agreement of RASPT2 and CFM spectra with experiment, the RASPT2 calculation tends to underestimate the LF state energies compared to experiment and compared to the CFM and RAS calculations from ref 68 by 10−20%. First, this mismatch of the calculated RASPT2 LF state energies could be attributed to the exclusion of vibrational effects in the calculation. Optical transitions are generally accompanied by vibrational excitations, causing the central energy of experimental peaks to shift toward higher energies. In the UV−vis spectrum of the $[Ni(H_2O)_6]^{2+}$ complex, the peaks are shifted by 0.1−0.2 eV compared to pure electronic transitions.[69] One could expect vibrational shifts of similar magnitude in the RIXS spectra, explaining the discrepancy between RIXS calculation and experiment. There are important differences between the vibrational effects in UV−vis and RIXS spectroscopy, though, which are discussed in the next section. Note that the empirical parameters used in the CFM calculation account for the vibrational effects as calculated peak positions are effectively adjusted to the experimental positions. The second cause for the mismatch between measured and calculated RASPT2 LF state energies could be attributed to the insufficient inclusion of the dynamical correlations by the PT2 method with the current choice of active space. This could also explain the differences between the RASPT2 and RAS calculations.[68]

Our assignments in Table 1 differ from the results in ref 28, which can be explained by the inconsistencies introduced when using one-electron models such as those used in ref 28 in contrast to the many-electron approach applied here. It is well-known that a many-electron description is necessary to interpret the metal L-edge XA and RIXS spectral features of TM compounds.[35,70,71]

In ligand-field theory, the LF state energies are determined by $10Dq$ and the Racah parameters B and C (not considering the 3d spin−orbit interaction). In addition to $10Dq$, we can also uniquely determine the values of the Racah parameters. We utilized the following formula from ref 9 to calculate B and C (state energies are with respect to the ground state $^3A_{2g}$):

$$B = \frac{E(^3T_{1g}(P))^2 - 30Dq\,E(^3T_{1g}(P)) + 200Dq^2}{15E(^3T_{1g}(P)) - 270Dq} \quad (1)$$

$$C = 0.5E(^1T_{1g}(G)) - 6B - 5Dq \quad (2)$$

For quantitative comparison we also derived these parameters from the RASPT2 and CFM calculations. In the CFM calculation, $10Dq$ and the Coulomb repulsion parameters are actually input parameters, and we used here the experimental value of 1.1 eV for $10Dq$; the Slater integrals F_2 and F_4 were calculated at the Hartree−Fock level and scaled by an empirical factor of 0.8 (the Slater integrals are related to the Racah parameters by the following equations: $F_2 = 49B + C$ and $F_4 = 63/5C$).

As accurate ab initio calculations of the Coulomb repulsion parameters are generally still a challenge, we are particularly interested in comparing the values of B and C as derived from the RASPT2 calculation to the experimental and CFM values. The results are summarized in Table 2. The ab initio RASPT2 values are off by 10−30%, similar to the respective energies of the LF states in Table 1. The parameters derived from the RIXS experiment match very well with the UV−vis results.

Table 2. Electronic Structure Parameters of the $[Ni(H_2O)_6]^{2+}$ Complex Which Determine the Energetic Positions of the LF States[a]

	RIXS expt. this work (eV)	UV−vis expt.[69] (eV)	RASPT2 theory this work (eV)	CFM theory this work (eV)	(CFM-RASPT2)/CFM (eV)
$10Dq$	1.1	1.1	0.9	1.1	18%
B	0.13	0.12	0.11	0.13	12%
C	0.42	0.47	0.61	0.48	−27%

[a]The experimental UV−vis results are taken from ref 69.

dx.doi.org/10.1021/jp4100813 | J. Phys. Chem. B 2013, 117, 16512−16521

Comparison of RIXS and UV−Vis Absorption Spectroscopy. While in UV−vis absorption spectroscopy only single-dipole transitions contribute to the spectrum, the RIXS process is described by a scattering process (two dipole transitions) through an intermediate state involving the highly localized atomic core orbital.

In the optical absorption spectrum, transitions to LF states are by a factor of 1/1000 weaker than strong CT and ligand-centered absorption peaks.[8] This is because in octahedral TM complexes direct optical dipole transitions between the different LF states are Laporte forbidden and spin-allowed transitions have noticeable oscillator strengths due to dynamical distortions (vibronic coupling).[69] In contrast, RIXS transitions to the LF states are allowed in octahedral TM complexes and the RIXS spectrum is typically dominated by the LF features.

The UV−vis absorption spectrum of $[Ni(H_2O)_6]^{2+}$ as adapted from ref 69 is displayed in Figure 6. Comparison

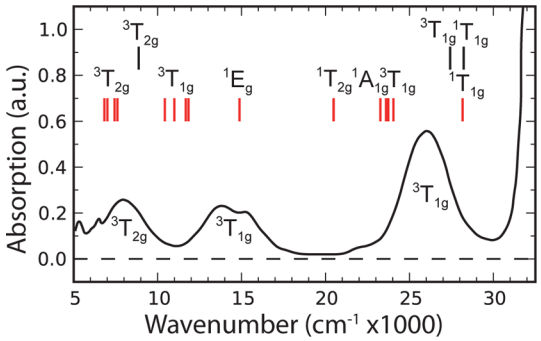

Figure 6. Experimental UV−vis absorption spectrum from ref 69 (black solid line) compared with the energies of the LF states deduced from the L_3-RIXS experiment (black sticks) and from the RASPT2 calculation (red sticks; same energies and states as in Figure 2b).

with the RIXS spectra in Figure 5 reveals some important differences between these techniques. First, starting from the A_{2g} ground state of $[Ni(H_2O)_6]^{2+}$ the allowed direct (single-dipole) transitions are only to T_{2u} states, whereas the RIXS scattering selection rules allow transitions to final states with A_{2g}, E_g, T_{1g}, and T_{2g} symmetry. Second, the spin selection rule is well-preserved in UV−vis absorption. As the 3d spin−orbit coupling is weak, only dipole transitions which preserve the spin have intensity in the UV−vis spectrum of $[Ni(H_2O)_6]^{2+}$, and starting from $^3A_{2g}$ only triplet states are reached (Figure 6). The 2p spin−orbit coupling, however, is the dominant interaction in the core-excited intermediate state in Ni L-edge RIXS (stronger than LF and 2p−3d direct and exchange Coulomb interactions). Therefore, spin is not a good quantum number for the intermediate states, and depending on the selected intermediate state, LF final states with spin multiplicity different than that of the ground state can have similar RIXS intensities. For Ni L-edge RIXS of $[Ni(H_2O)_6]^{2+}$ this allows probing singlet final states. One example for this is the peak at 3.5 eV energy transfer at XA resonance B corresponding to the $^1T_{1g}$ final state (Figure 5c). Third, the possibility to tune the incident photon energy to resonantly select particular intermediate states adds an extra dimension to RIXS as relative intensities of the final states depend strongly on the chosen X-ray absorption resonance. We utilized this here to determine the energies of the closely lying $^3T_{1g}$ and $^1T_{1g}$ LF states at energy transfers of 3.4 and 3.5 eV, respectively. Their separation of only 0.1 eV is well below our experimental resolution. However, tuning to resonances A and B enhances the intensities of $^3T_{1g}$ and $^1T_{1g}$, respectively, as $^1T_{1g}$ cannot be reached when exciting at resonance A and allows for their separate investigation.

Finally, the direct comparison of UV−vis and RIXS results in Figure 6 shows that the LF-state energies do not exactly match: the energies of the $^3T_{2g}$ and $^3T_{1g}$ states as measured with RIXS are shifted to higher energies with respect to the corresponding UV−vis absorption peaks. Such an observation was made also in the comparison of UV−vis and L-edge RIXS results of cobalt compounds in ref 72. We believe that these discrepancies can be explained by considering the vibrational effects. The vibrational effects in the UV−vis spectrum of the $[Ni(H_2O)_6]^{2+}$ complex were simulated in ref 69, and similar to the mismatch of RIXS with the calculations, we believe that the blue shift of the RIXS energies compared to the UV−vis energies can be attributed to differences of vibrational effects in the respective methods. Qualitatively one can outline these differences of vibrational effects on spectral peak positions and shapes between UV−vis and RIXS. First, in the case of a nominally octahedral complex, UV−vis spectroscopy probes preferably distorted configurations, whereas RIXS in contrast can probe also strictly nondistorted (octahedral) configurations. Second, intermediate core-exited states in RIXS are generally vibrationally highly excited, and this allows reaching higher vibrational states in the electronic final state compared to UV−vis spectroscopy. Therefore, extended vibrational progressions appear in the RIXS spectrum and we expect this to lead to larger effective vibrational energy shifts. A quantitative evaluation of these effects would be desirable. However, this requires the calculation of numerous multidimensional potential energy surfaces, including the core-excited states, and the subsequent calculation of nuclear wave functions.[39] The RASPT2 method provides a suitable computational framework for this, but it goes beyond the scope of the present investigation.

CONCLUSIONS

We investigated electronic structure of the archetypical hexaaqua complex $[Ni(H_2O)_6]^{2+}$ with an unprecedented combination of resonant inelastic soft X-ray scattering (RIXS) measurements and ab initio calculations at the Ni L absorption edge. The RIXS spectra directly reflect the relative energies of the ligand-field and charge-transfer valence-excited states of the complex and give element-specific access to the ground-state electronic structure of the complex. The results allow for determining the ligand-field strength $10Dq$ and 3d−3d Coulomb repulsion in $[Ni(H_2O)_6]^{2+}$. The $10Dq$ = 1.1 eV estimate and the Racah parameters B = 0.13 eV and C = 0.42 eV characterizing 3d−3d Coulomb interactions as derived from the measured ligand-field state energies compare very well with the results from UV−vis spectroscopy. These results show in general how L-edge RIXS can be used to complement existing spectroscopic tools for the investigation of bonding in 3d transition-metal coordination compounds in solution.

We have also demonstrated for the $[Ni(H_2O)_6]^{2+}$ complex that a full simulation of Ni L-edge RIXS is feasible within a novel RASPT2 computational scheme. Analysis of the RASPT2 results showed that the electronic structure parameters $10Dq$, B, and C agree with experiment to within 20%. These discrepancies are mostly a result of the vibrational effects not included in the calculation and are not due to errors in calculating the electronic structure. Latter errors might be

dx.doi.org/10.1021/jp4100813 | J. Phys. Chem. B 2013, 117, 16512−16521

present because of only insufficient description of the dynamical correlation. The novel RASPT2 calculations are compared in detail to the results of more established semiempirical CFM calculations. This demonstrates that ab initio RASPT2 calculations can be considered as a valuable new tool for the analysis of 3d transition-metal L-edge spectroscopy. Note that the RASPT2 method, based on an LCAO-MO approach, can be used to provide considerably more insight than semiempirical CFM calculations into the bonding of TM complexes.

We believe that L-edge RIXS combined with ab initio RASPT2 calculations can be utilized to resolve complex questions regarding bonding and chemistry of TM compounds, therefore contributing to the understanding of their catalytic and photoactive properties.

■ ASSOCIATED CONTENT

Supporting Information

Addition details regarding assignments of the experimental and calculated spectral features and determination of the experimental peak positions. This material is available free of charge via the Internet at http://pubs.acs.org.

■ AUTHOR INFORMATION

Corresponding Author

*E-mail: wernet@helmholtz-berlin.de. Phone: +49 30 806213448. Fax: +49 30 806212114.

Notes

The authors declare no competing financial interest.

■ ACKNOWLEDGMENTS

We gratefully acknowledge the continuous support by the BESSYII staff. Portions of the presented research were funded by the Helmholtz Virtual Institute "Dynamic Pathways in Multidimensional Landscapes". This work was supported by the Swedish Research Council.

■ REFERENCES

(1) Werner, A. Beitrag zur Konstitution anorganischer Verbindungen. *Zeitschrift für Anorganische Chemie* **1893**, *3*, 267−330.

(2) Kallies, B.; Meier, R. Electronic Structure of 3d $M(H_2O)_6^{3+}$ Ions from Sc^{III} to Fe^{III}: A Quantum Mechanical Study Based on DFT Computations and Natural Bond Orbital Analyses. *Inorg. Chem.* **2001**, *40*, 3101−3112.

(3) Erras-Hanauer, H.; Clark, T.; van Eldik, R. Molecular Orbital and DFT Studies on Water Exchange Mechanisms of Metal Ions. *Coord. Chem. Rev.* **2003**, *238*, 233−253.

(4) Helm, L.; Merbach, A. E.Water Exchange on Metal Ions: Experiments and Simulations. *Coord. Chem. Rev.* **1999**, *187*, 151−181.

(5) Iuchi, S.; Morita, A.; Kato, S. Potential Energy Surfaces and Dynamics of Ni^{2+} Ion Aqueous Solution: Molecular Dynamics Simulation of the Electronic Absorption Spectrum. *J. Chem. Phys.* **2004**, *121*, 8446−8457.

(6) Deguillaume, L.; Leriche, M.; Desboeufs, K.; Mailhot, G.; George, C.; Chaumerliac, N. Transition Metals in Atmospheric Liquid Phases: Sources, Reactivity, and Sensitive Parameters. *Chem. Rev.* **2005**, *105*, 3388−3431.

(7) Ohtaki, H.; Radnai, T. Structure and Dynamics of Hydrated Ions. *Chem. Rev.* **1993**, *93*, 1157−1204.

(8) Figgis, B. N.; Hitchman, M. A. *Ligand Field Theory and Its Applications*; Wiley-VCH: New York, 2000.

(9) Griffith, J. S. *The Theory of Transition-Metal Ions*; Cambridge University Press: Cambridge, U.K., 1961.

(10) Tanabe, Y.; Sugano, S. On the Absorption Spectra of Complex Ions. I. *J. Phys. Soc. Jpn.* **1954**, *9*, 753−766.

(11) Tanabe, Y.; Sugano, S. On the Absorption Spectra of Complex Ions. II. *J. Phys. Soc. Jpn.* **1954**, *9*, 766−779.

(12) Stöhr, J. *NEXAFS Spectroscopy*; Springer: Berlin, 1992.

(13) Aziz, E. F. The Solvation of Ions and Molecules Probed via Soft X-ray Spectroscopies. *J. Electron Spectrosc. Relat. Phenom.* **2010**, *177*, 168−180.

(14) Aziz, E. F.; Eisebitt, S.; de Groot, F.; Chiou, J. W.; Dong, C. G.; Guo, J. H.; Eberhardt, W. Direct Contact versus Solvent-Shared Ion Pairs in $NiCl_2$ Electrolytes Monitored by Multiplet Effects at Ni(II) L Edge X-ray Absorption. *J. Phys. Chem. B* **2007**, *111*, 4440−4445.

(15) Aziz, E. F.; Rittmann-Frank, M. H.; Lange, K. M.; Bonhommeau, S.; Chergui, M. Charge Transfer to Solvent Identified Using Dark Channel Fluorescence-Yield L-Edge Spectroscopy. *Nat. Chem.* **2010**, *2*, 853−857.

(16) Bonhommeau, S.; Ottosson, N.; Pokapanich, W.; Svensson, S.; Eberhardt, W.; Björneholm, O.; Aziz, E. F. Solvent Effect of Alcohols at the L-Edge of Iron in Solution: X-ray Absorption and Multiplet Calculations. *J. Phys. Chem. B* **2008**, *112*, 12571−12574.

(17) Schreck, S.; Gavrila, G.; Weniger, C.; Wernet, Ph. A Sample Holder for Soft X-ray Absorption Spectroscopy of Liquids in Transmission Mode. *Rev. Sci. Instrum.* **2011**, *82*, 103101.

(18) Näslund, L. A.; Cavalleri, M.; Ogasawara, H.; Nilsson, A.; Pettersson, L. G. M.; Wernet, Ph.; Edwards, D. C.; Sandström, M.; Myneni, S. Direct Evidence of Orbital Mixing Between Water and Solvated Transition-Metal Ions: An Oxygen 1s XAS and DFT Study of Aqueous Systems. *J. Phys. Chem. A* **2003**, *107*, 6869−6876.

(19) Gotz, M. D.; Soldatov, M. A.; Lange, K. M.; Engel, N.; Golnak, R.; Könnecke, R.; Atak, K.; Eberhardt, W.; Aziz, E. F. Probing Coster−Kronig Transitions in Aqueous Fe^{2+} Solution Using Inverse Partial and Partial Fluorescence Yield at the L-Edge. *J. Phys. Chem. Lett.* **2012**, *3*, 1619−1623.

(20) Huse, N.; Cho, H.; Hong, K.; Jamula, L.; de Groot, F. M. F.; Kim, T. K.; Mc-Cusker, J. K.; Schoenlein, R. W. Femtosecond Soft X-ray Spectroscopy of Solvated Transition-Metal Complexes: Deciphering the Interplay of Electronic and Structural Dynamics. *J. Phys. Chem. Lett.* **2011**, *2*, 880−884.

(21) Huse, N.; Kim, T. K.; Jamula, L.; McCusker, J. K.; de Groot, F. M. F.; Schoenlein, R. W. Photo-Induced Spin-State Conversion in Solvated Transition Metal Complexes Probed via Time-Resolved Soft X-ray Spectroscopy. *J. Am. Chem. Soc.* **2010**, *132*, 6809−6816.

(22) Soldatov, M. A.; Lange, K. M.; Gotz, M. D.; Engel, N.; Golnak, R.; Kothe, A.; Aziz, E. F. On the Origin of Dips in Total Fluorescence Yield X-ray Absorption Spectra: Partial and Inverse Partial Fluorescence Yield at the L-edge of Cobalt Aqueous Solution. *Chem. Phys. Lett.* **2012**, *546*, 164−167.

(23) Winter, B.; Faubel, M. Photoemission from Liquid Aqueous Solutions. *Chem. Rev.* **2006**, *106*, 1176−1211.

(24) Seidel, R.; Ghadimi, S.; Lange, K. M.; Bonhommeau, S.; Soldatov, M. A.; Golnak, R.; Kothe, A.; Köonnecke, R.; Soldatov, A.; Thürmer, S.; et al. Origin of Dark-Channel X-ray Fluorescence from Transition-Metal Ions in Water. *J. Am. Chem. Soc.* **2012**, *134*, 1600−1605.

(25) Seidel, R.; Thürmer, S.; Moens, J.; Geerlings, P.; Blumberger, J.; Winter, B. Valence Photoemission Spectra of Aqueous $Fe^{2+/3+}$ and $[Fe(CN)_6]^{4-/3-}$ and Their Interpretation by DFT Calculations. *J. Phys. Chem. B* **2011**, *115*, 11671−11677.

(26) Seidel, R.; Thürmer, S.; Winter, B. Photoelectron Spectroscopy Meets Aqueous Solution: Studies from a Vacuum Liquid Microjet. *J. Phys. Chem. Lett.* **2011**, *2*, 633−641.

(27) Thürmer, S.; Seidel, R.; Eberhardt, W.; Bradforth, S. E.; Winter, B. Ultrafast Hybridization Screening in Fe^{3+} Aqueous Solution. *J. Am. Chem. Soc.* **2011**, *133*, 12528−12535.

(28) Lange, K. M.; Könnecke, R.; Ghadimi, S.; Golnak, R.; Soldatov, M. A.; Hodeck, K. F.; Soldatov, A.; Aziz, E. F. High Resolution X-ray Emission Spectroscopy of Water and Aqueous Ions Using the Micro-Jet Technique. *Chem. Phys.* **2010**, *377*, 1−5.

(29) Lange, K. M.; Kothe, A.; Aziz, E. F. Chemistry in Solution: Recent Techniques and Applications Using Soft X-ray Spectroscopy. *Phys. Chem. Chem. Phys.* **2012**, *14*, 5331−5338.

(30) Wernet, Ph.; Kunnus, K.; Schreck, S.; Quevedo, W.; Kurian, R.; Techert, S.; de Groot, F. M. F.; Odelius, M.; Föhlisch, A. Dissecting Local Atomic and Intermolecular Interactions of Transition-Metal Ions in Solution with Selective X-ray Spectroscopy. *J. Phys. Chem. Lett.* **2012**, *3*, 3448−3453.
(31) Kunnus, K.; Rajkovic, I.; Schreck, S.; Quevedo, W.; Eckert, S.; Beye, M.; Suljoti, E.; Weniger, C.; Kalus, C.; Grübel, S.; et al. A Setup for Resonant Inelastic Soft X-ray Scattering on Liquids at Free Electron Laser Light Sources. *Rev. Sci. Instrum.* **2012**, *83*, 123109.
(32) Suljoti, E.; Garcia-Diez, R.; Bokarev, S. I.; Lange, K. M.; Schoch, R.; Dierker, B.; Dantz, M.; Yamamoto, K.; Engel, N.; Atak, K.; et al. Direct Observation of Molecular Orbital Mixing in a Solvated Organometallic Complex. *Angew. Chem., Int. Ed.* **2013**, *52*, 9841−9844.
(33) Atak, K.; Bokarev, S. I.; Gotz, M.; Golnak, R.; Lange, K. M.; Engel, N.; Dantz, M.; Suljoti, E.; Kühn, O.; Aziz, E. F. Nature of the Chemical Bond of Aqueous Fe^{2+} Probed by Soft X-ray Spectroscopies and ab Initio Calculations. *J. Phys. Chem. B* **2013**, *117*, 12613−12618.
(34) Ament, L. J. P.; van Veenendaal, M.; Devereaux, T. P.; Hill, J. P.; van den Brink, J. Resonant Inelastic X-ray Scattering Studies of Elementary Excitations. *Rev. Mod. Phys.* **2011**, *83*, 705−767.
(35) de Groot, F. M. F. High-Resolution X-ray Emission and X-ray Absorption Spectroscopy. *Chem. Rev.* **2001**, *101*, 1779−1808.
(36) Föhlisch, A.; Hasselström, J.; Bennich, P.; Wassdahl, N.; Karis, O.; Nilsson, A.; Triguero, L.; Nyberg, M.; Pettersson, L. G. M. Ground-State Interpretation of X-ray Emission Spectroscopy on Adsorbates: CO Adsorbed on Cu(100). *Phys. Rev. B* **2000**, *61*, 16229−16240.
(37) Ågren, H.; Luo, Y.; Gel'mukhanov, F.; Jensen, H. J. A. Screening in Resonant X-ray Emission of Molecules. *J. Electron Spectrosc. Relat. Phenom.* **1996**, *82*, 125−134.
(38) Gel'mukhanov, F.; Ågren, H. Raman, Non-Raman, and Anti-Raman Dispersion in Resonant X-ray Scattering Spectra of Molecules. *Phys. Rev. A* **1996**, *54*, 3960−3970.
(39) Gel'mukhanov, F.; Ågren, H. Resonant X-ray Raman Scattering. *Phys. Rep.* **1999**, *312*, 87−330.
(40) de Groot, F. M. F.; Arrio, M. A.; Sainctavit, P.; Cartier, C.; Chen, C. T. Fluorescence Yield Detection: Why It Does Not Measure the X-ray Absorption Cross Section. *Solid State Commun.* **1994**, *92*, 991−995.
(41) Ghiringhelli, G.; Matsubara, M.; Dallera, C.; Fracassi, F.; Gusmeroli, R.; Piazzalunga, A.; Tagliaferri, A.; Brookes, N. B.; Kotani, A.; Braicovich, L. NiO As a Test Case for High Resolution Resonant Inelastic Soft X-ray Scattering. *J. Phys.: Condens. Matter* **2005**, *17*, 5397−5412.
(42) de Groot, F. M. F.; Fuggle, J. C.; Thole, B. T.; Sawatzky, G. A. 2*p* X-Ray Absorption of 3*d* Transition-Metal Compounds: An Atomic Multiplet Description Including the Crystal-Field. *Phys. Rev. B* **1990**, *42*, 5459−5468.
(43) Thole, B. T.; van der Laan, G.; Fuggle, J. C.; Sawatzky, G. A.; Karnatak, R. C.; Esteva, J.-M. 3d X-ray Absorption Lines and the $3d^9 4f^{n+1}$ Multiplets of the Lanthanides. *Phys. Rev. B* **1985**, *32*, 5107−5118.
(44) Haverkort, M. W.; Zwierzycki, M.; Andersen, O. K. Multiplet Ligand-Field Theory Using Wannier Orbitals. *Phys. Rev. B* **2012**, *85*, 165113.
(45) Agui, A.; Uozumi, T.; Mizumaki, M.; Kääambre, T. Intermetallic Charge Transfer in $FeTiO_3$ Probed by Resonant Inelastic Soft X-ray Scattering. *Phys. Rev. B* **2009**, *79*, 092402.
(46) Roemelt, M.; Maganas, D.; DeBeer, S.; Neese, F. A Combined DFT and Restricted Open-Shell Configuration Interaction Method Including Spin-Orbit Coupling: Application to Transition Metal L-edge X-ray Absorption Spectroscopy. *J. Chem. Phys.* **2013**, *138*, 204101.
(47) Roemelt, M.; Neese, F. Excited States of Large Open-Shell Molecules: An Eficient, General, and Spin-Adapted Approach Based on a Restricted Open-Shell Ground State Wave function. *J. Phys. Chem. A* **2013**, *117*, 3069−3083.
(48) Ikeno, H.; Tanaka, I.; Koyama, Y.; Mizoguchi, T.; Ogasawara, K. First-Principles Multielectron Calculations of Ni $L_{2,3}$ NEXAFS and ELNES for $LiNiO_2$ and Related Compounds. *Phys. Rev. B* **2005**, *72*, 075123.
(49) Ikeno, H.; Mizoguchi, T.; Tanaka, I. Ab initio Charge Transfer Multiplet Calculations on the $L_{2,3}$ XANES and ELNES of 3*d* Transition Metal Oxides. *Phys. Rev. B* **2011**, *83*, 155107.
(50) Vinson, J.; Rehr, J. J.; Kas, J. J.; Shirley, E. L. Bethe-Salpeter Equation Calculations of Core Excitation Spectra. *Phys. Rev. B* **2011**, *83*, 115106.
(51) Vinson, J.; Rehr, J. J. Ab initio Bethe-Salpeter Calculations of the X-ray Absorption Spectra of Transition Metals at the L-Shell Edges. *Phys. Rev. B* **2012**, *86*, 195135.
(52) Josefsson, I.; Kunnus, K.; Schreck, S.; Föhlisch, A.; de Groot, F. M. F.; Wernet, Ph.; Odelius, M. Ab initio Calculations of X-ray Spectra: Atomic Multiplet and Molecular Orbital Effects in a Multiconfigurational SCF Approach to the L-Edge Spectra of Transition Metal Complexes. *J. Phys. Chem. Lett.* **2012**, *3*, 3565−3570.
(53) Bokarev, S. I.; Dantz, M.; Suljoti, E.; Kühn, O.; Aziz, E. F. State-Dependent Electron Delocalization Dynamics at the Solute-Solvent Interface: Soft-X-Ray Absorption Spectroscopy and Ab Initio Calculations. *Phys. Rev. Lett.* **2013**, *111*, 083002.
(54) Magini, M. Hydration and Complex Formation Study on Concentrated MCl_2 Solutions [M=Co(II), Ni(II), Cu(II)] by X-ray Diffraction Technique. *J. Chem. Phys.* **1981**, *74*, 2523−2529.
(55) Waizumi, K.; Kouda, T.; Tanio, A.; Fukushima, N.; Ohtaki, H. Structural Studies on Saturated Aqueous Solutions of Manganese(II), Cobalt(II), and Nickel(II) Chlorides by X-ray Diffraction. *J. Solution Chem.* **1999**, *28*, 83−100.
(56) Aquilante, F.; De Vico, L.; Ferre, N.; Ghigo, G.; Malmqvist, P. A.; Neogrady, P.; Pedersen, T. B.; Pitonak, M.; Reiher, M.; Roos, B. O.; et al. Software News and Update MOLCAS 7: The Next Generation. *J. Comput. Chem.* **2010**, *31*, 224−247.
(57) Roos, B. O.; Lindh, R.; Malmqvist, P. A.; Veryazov, V.; Widmark, P. O. Main Group Atoms and Dimers Studied with a New Relativistic ANO Basis Set. *J. Phys. Chem. A* **2004**, *108*, 2851−2858.
(58) Roos, B. O.; Lindh, R.; Malmqvist, P. A.; Veryazov, V.; Widmark, P. O. New Relativistic ANO Basis Sets for Transition Metal Atoms. *J. Phys. Chem. A* **2005**, *109*, 6575−6579.
(59) Douglas, M.; Kroll, N. M. Quantum Electrodynamical Corrections to Fine-Structure of Helium. *Ann. Phys.* **1974**, *82*, 89−155.
(60) Hess, B. A. Relativistic Electronic-Structure Calculations Employing a 2-component No-Pair Formalism with External-Field Projection Operators. *Phys. Rev. A* **1986**, *33*, 3742−3748.
(61) Malmqvist, P. A.; Rendell, A.; Roos, B. O. The Restricted Active Space Self-Consistent-Field Method, Implemented with a Split Graph Unitary-Group Approach. *J. Phys. Chem.* **1990**, *94*, 5477−5482.
(62) Finley, J.; Malmqvist, P. A.; Roos, B. O.; Serrano-Andres, L. The Multi-State CASPT2 Method. *Chem. Phys. Lett.* **1998**, *288*, 299−306.
(63) Malmqvist, P. A.; Roos, B. O.; Schimmelpfennig, B. The Restricted Active Space (RAS) State Interaction Approach with Spin-Orbit Coupling. *Chem. Phys. Lett.* **2002**, *357*, 230−240.
(64) Kurian, R.; Kunnus, K.; Wernet, Ph.; Butorin, S. M.; Glatzel, P.; de Groot, F. M. F. Intrinsic Deviations in Fluorescence Yield Detected X-ray Absorption Spectroscopy: The Case of the Transition Metal $L_{2,3}$ Edges. *J. Phys.: Condens. Matter* **2012**, *24*, 452201.
(65) Krause, M. Atomic Radiative and Radiationless Yield for K and L Shells. *J. Phys. Chem. Ref. Data* **1979**, *8*, 307−327.
(66) Kunnus, K.; Josefsson, I.; Schreck, S.; Quevedo, W.; Miedema, P. S.; Techert, S.; de Groot, F. M. F.; Föhlisch, A.; Odelius, M.; Wernet, Ph. Unpublished work.
(67) Coster, D.; Kronig, R. D. L. New Type of Auger Effect and Its Influence on the X-ray Spectrum. *Physica* **1935**, *2*, 13−24.
(68) Casanova, D.; Head-Gordon, M. Restricted Active Space Spin-Flip Configuration Interaction Approach: Theory, Implementation and Examples. *Phys. Chem. Chem. Phys.* **2009**, *11*, 9779−9790.
(69) Landry-Hum, J.; Bussiere, G.; Daniel, C.; Reber, C. Triplet Electronic States in d^2 and d^8 Complexes Probed by Absorption

Spectroscopy: A CASSCF/CASPT2 Analysis of $[V(H_2O)_6]^{3+}$ and $[Ni(H_2O)_6]^{2+}$. *Inorg. Chem.* **2001**, *40*, 2595−2601.
(70) de Groot, F.; Kotani, A. *Core Level Spectroscopy of Solids*; CRC Press: Boca Raton, FL, 2008.
(71) de Groot, F. M. F. Multiplet Effects in X-ray Spectroscopy. *Coord. Chem. Rev.* **2005**, *249*, 31−63.
(72) van Schooneveld, M. M.; Gosselink, R. W.; Eggenhuisen, T. M.; Al Samarai, M.; Monney, C.; Zhou, K. J.; Schmitt, T.; de Groot, F. M. F. A Multispectroscopic Study of 3d Orbitals in Cobalt Carboxylates: The High Sensitivity of 2p3d Resonant X-ray Emission Spectroscopy to the Ligand Field. *Angew. Chem., Int. Ed.* **2013**, *52*, 1170−1174.